Spectrum Utilization Efficiency Analysis in 3D UAV Networks

Kasun Prabhath and Sudharman K. Jayaweera
CISL, ECE Department, University of New Mexico, Albuquerque, NM, USA.
Email: prabhathgwk@unm.edu, jayaweera@unm.edu

MILCOM 2024 - 2024 IEEE Military Communications Conference (MILCOM) | 979-8-3503-7423-0/24/$31.00 ©2024 IEEE | DOI: 10.1109/MILCOM61039.2024.10773958

***Abstract*—This paper investigates the Spectrum Utilization Efficiency (SUE) and average link Spectral Efficiency (SE) of 3D communication systems comprised of Unmanned Aerial Vehicles (UAVs). In particular, we characterize the impact of key parameters such as frequency reuse cell radius, normalized frequency reuse distance, and path-loss exponent on the SUE and SE of systems in 3D space. We derive analytical expressions for SUE and SE under both free-space and log-normal pathloss models and validate them through simulations. Our results indicate that while increasing the normalized frequency reuse distance decreases SUE, it improves the average link SE. Furthermore, smaller cell radii or larger pathloss exponents can improve SUE, offering important insights for optimizing frequency reuse strategies in UAV-based networks in 3D space. This study lays the groundwork for future exploration of spectrum management and dynamic spectrum sharing (DSS) in dynamic and complex integrated aerial and ground communication environments.**

***Index Terms*—Aerial communications, frequency reuse planning, spectrum management**

I. Introduction

The electromagnetic spectrum, the essential medium for wireless communication, supports various technologies that society relies on, cellular networks, satellite communication, 5G, autonomous vehicles, smart cities, and Internet of Things (IoT) [1]. As the spectrum is a finite resource and demand for it is rising rapidly, optimizing its use is essential. Effective spectrum utilization ensures the seamless coexistence of diverse technologies without harmful interference and accommodates more users within the same frequency band, driving technological innovation, enhancing connectivity, and fostering economic growth. The importance of efficient spectrum utilization in three-dimensional (3D) space is exemplified with the introduction of technologies such as Unmanned Aerial Vehicles (UAV) with Next Generation Node B (gNBs), High Altitude Platform Stations (HAPS) gNBs, and Non-Terrestrial Networks (NTN) as part of 5G Advanced (5G-Adv) and future 6G systems [2]. These technologies operate in 3D space, making efficient spectrum use even more critical.

Link spectral efficiency (SE), measured in bit/s/Hz, is a widely used metric in communication systems that defines the information rate of a communication link over a given bandwidth. It focuses on the efficiency of the modulation and coding schemes used in a communication system. However, we are interested in a measure that evaluates how effectively the spectrum is utilized in space and time by a particular system. While link SE provides important insights into the efficiency of physical layer of a communication link, it does not provide a sufficient characterization of the dependency of spectrum usage on geographical spacing, frequency reuse and time sharing.

Spectrum utilization efficiency (SUE) measures how effectively the available frequency spectrum is used in a communication system [3]. Efficient spectrum use can be achieved through geographical spacing, frequency sharing, orthogonal frequency use, and time-sharing or division. In traditional 2D systems, SUE in a communication system is defined as the information transfer rate per unit bandwidth used and unit effective area. This measure accounts for the frequency reuse method when calculating the efficiency of spectrum utilization in a communication system.

Recent research has introduced few new concepts for spectrum management and frequency reuse in wireless networks in 3D space. For example, [1] proposes a comprehensive UAV-based 3D cellular network model, incorporating UAV-user equipment (UE), UAV-gNBs, and HAPS UAVs, using truncated octahedron cells for optimal placement and frequency planning to reduce latency and improve spectral efficiency. On the other hand, [4] focuses on link SE of 3D networks, modeling UAV-UE spatial distribution with a 3D Binomial Point Process and employing stochastic geometry for coverage probability analysis. Additionally, a 3D frequency reuse architecture for UAV swarms in [5] extends traditional 2D models to 3D, using covariance matrices to determine 3D volume coverage, and proposes an algorithm for spectrum management. These studies collectively demonstrate possible frequency reuse strategies for wireless networks in 3D space. However, they do not provide a systematic analysis of SUE of wireless networks in 3D space to glean insights into pros and cons of different frequency reuse strategies.

In this paper, the objective is to analytically characterize the SUE and link SE of UAV communication systems in 3D space where UAVs adapt their rate to physical channel and interference conditions. This analysis sheds light on how SUE and link SE depend on frequency reuse distance in 3D space. We start with the architecture for frequency reuse in 3D space proposed in [1], [5]. Based on this frequency

[1]This paper is based upon work supported by the National Science Foundation under grant no. NSF 2148178, and is supported in part by funds from federal agency and industry partners as specified in the Resilient & Intelligent NextG Systems (RINGS) program.

979-8-3503-7423-0/24/$31.00 ©2024 IEEE

reuse architecture, we derive analytical expressions for SUE and link SE of an aerial communication network in 3D space, considering both best and worst-case scenarios. We take into account the effect of random user locations and study the average SUE and link SE under different channel models with different propagation parameters. In particular, we consider the free-space propagation path loss model that is known to be applicable to high-altitude UAV networks [1] and the log-normal fading model that is suitable for low-altitude UAV operations [6]. For our analyses and simulations in this paper, we limit ourselves to downlink communications (UAV-gNB to UAV-UE users) in a fully loaded communication system (i.e., all available channels in each cell are fully utilized).

The remainder of the paper is organized as follows: Section II provides an in-depth discussion of the propagation model, frequency reuse model, assumptions, user location models, and the definitions of SUE and link SE. Section III derives analytical expressions for SUE and link SE under the pathloss model. In Section IV, we extend the analysis to the log-normal pathloss model. Section V details the simulation results and key findings. Finally, Section VI offers concluding remarks.

II. System Model

This section describes our assumptions regarding the 3D aerial cellular system and co-channel interference. We then detail the distribution of the user signal-to-interference-plus-noise ratio (SINR) based on the assumed propagation channel and user location models. Finally, we define link SE and SUE of a communication system.

A. Geometric Model for 3D Frequency Reuse

Traditionally, in 2D, base station coverage is assumed to be a circular region that can be modeled by a hexagon. In 3D, the base station coverage volume can be assumed to be a sphere. The geometric modeling for 3D frequency reuse is explored in [5], which highlights the use of polyhedra for efficient tessellation.

1) Truncated Octahedron Tessellation: The work in [5] proposes a 3D geometric model for frequency reuse based on truncated octahedron tessellation. This polyhedron, with 6 square faces and 8 hexagonal faces, is used for optimal space tessellation. The initial truncated octahedron is centered at the origin, with a vertex distance of R. The tessellation is achieved through specific geometric translations to ensure seamless coverage.

2) Lattice Tessellation: The first lattice tessellation shifts the original truncated octahedron cell by multiples of $\frac{2R}{\sqrt{5}}[2,0,0]$, $\frac{2R}{\sqrt{5}}[0,2,0]$, and $\frac{2R}{\sqrt{5}}[0,0,2]$. The second lattice tessellation introduces an additional displacement by $\frac{2R}{\sqrt{5}}[1,1,1]$.

3) Frequency Reuse Cluster Size: To reduce co-channel interference and improve SINR, the frequency reuse cluster size in 3D systems is determined using the derived distances between the centers of adjacent truncated octahedrons. The co-channel distance, when cells are connected through their

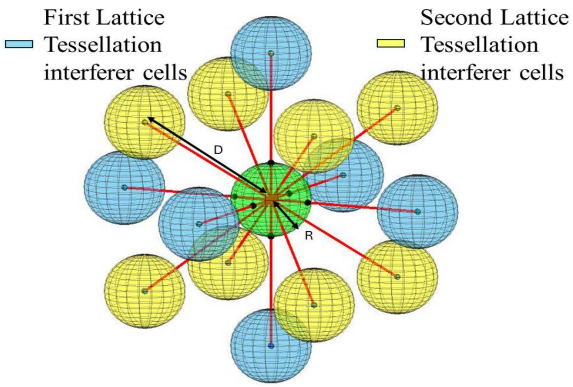

Fig. 1: Desired and co-channel cells in a 3D frequency reuse system, highlighting worst-case scenario user locations (indicated by black points)

hexagonal surfaces (D_h) and square surfaces (D_s), is respectively expressed as: $D_h = 2\sqrt{3/5}R_l$ and $D_s = 4/\sqrt{5}R_l$ where R_l is the radius of a larger truncated octahedron encompassing a cluster of cells. The cluster size N is determined by the volume ratio of the large truncated octahedron to a single cell, simplified using D_h and D_s:

$$N = \frac{5\sqrt{5}D_h^3}{24\sqrt{3}R^3} = \frac{5\sqrt{5}D_s^3}{64R^3}.$$

Unlike the 2D frequency reuse model, as shown in Fig. 1, the 3D frequency reuse model has 14 first-tier co-channels positioned according to the truncated octahedron lattice tessellation leading to two distinct frequency reuse distances. The cells corresponding to the first and second tessellations are represented by blue and yellow, respectively, in Fig. 1 while the desired UAV-gNB cell is shown in green. Although the truncated octahedron tessellation contains two distinct set of frequency reuse distances, for the sake of simplicity in calculations, in this paper we assume that all co-channel cells are at the same distance D from the desired UAV-gNB. A reasonable choice for common D can be $D = (6D_s + 8D_h)/14$.

B. Random User Distribution Model

For analytical convenience, we approximate the cell shape as a sphere with radius R. User locations are assumed to be uniformly distributed in the respective cell. Thus, the probability density function (PDF) of user location in spherical coordinates $\mathbf{r} = (r, \theta, \varphi)$ relative to the UAV-gNB is:

$$p(\mathbf{r}) = p(r, \theta, \varphi) = \frac{3r^2 \sin\theta}{4\pi(R^3 - R_0^3)} \tag{1}$$

where $r \in [R_0, R]$, $\theta \in [0, \pi]$ and $\varphi \in [0, 2\pi]$. The inner sphere radius R_0 corresponds to the closest distance the users can be from the UAV-gNB antenna [1].

C. Interference Analysis Model

To simplify the analysis, we assume interference-limited systems where thermal noise is negligible compared to co-channel interference [7]. Therefore, the SINR simplifies to signal-to-interference ratio (SIR), expressed as:

$$\gamma = \frac{S_D(r)}{S_I} = \frac{S_D(r)}{\sum_{i=1}^{N_I} S_i(r_i)} \tag{2}$$

where $S_D(r)$ is the received signal power at distance r from the desired UAV-gNB, S_I is the total interference power and $S_i(r_i)$ is the interfering signal power from the i-th interfering UAV-gNB located at distance r_i. Received signal power of a user at distance r from the desired UAV-gNB is:

$$S_D(r) = P_0 G_r G_t 10^{-PL(r)/10} \tag{3}$$

where P_0 is the transmit signal power, G_r is the receiver antenna gain, G_t transmit antenna gain and $PL(r)$ is the path loss (in dB) at a distance r. We assume that the total number of available channels, N_T, is fixed and equally distributed among the cells so that the number of channels per cell, N_c, is related to the frequency reuse cluster size as $N_c = N_T/N$. Based on the allocated set of channels, each UAV-gNB will allocate a channel or channels for each user based on availability. Hence, the achievable rate of the k-th user located at $\mathbf{r}$ can be written as

$$C_k = N_{c,k} B \log_2(1+\gamma_k) \tag{4}$$

where γ_k is the SIR of the k-th user at an arbitrary location $\mathbf{r}$ in a cell and $N_{c,k}$ is the number of channels allocated to the k-th user by the UAV-gNB. The average achievable rate of the k-th user can be written as

$$\bar{C}_k = N_{c,k} B \int_0^\infty \log_2(1+\gamma) P_{\gamma_k}(\gamma) d\gamma \tag{5}$$

where $P_{\gamma_k}(\gamma)$ is the probability density function (PDF) of γ_k conditioned on location $\mathbf{r}$. Since we assume that all users are distributed according to the same PDF, their SIR distribution $P_\gamma(\gamma)$ is also the same and thus, the average achievable rate for all users are also the same. Hence we can rewrite (5) as

$$\bar{C}_k = N_{c,k} B \int_0^\infty \log_2(1+\gamma) P_\gamma(\gamma) d\gamma \tag{6}$$

where γ is the SIR of a user.

D. Average Link Spectral Efficiency of Users

Link SE is an important metric for assessing the performance of communication systems, as it quantifies the average achievable data rate over a link per unit bandwidth. By evaluating link SE, system designers can understand how efficiently the available spectrum is utilized by individual users under different link conditions [1]. In UAV communication networks operating in 3D space, where users can experience highly variable channel conditions, understanding the average and worst-case link SE can be helpful in robust system design and spectrum management [1]. First, let the link SE of a user located at $\mathbf{r}$ be defined as the average achievable rate per unit bandwidth:

$$\eta_{SE}(\mathbf{r}) = \int_0^\infty \log_2(1+\gamma) P_\gamma(\gamma) d\gamma. \tag{7}$$

The *average link SE* can be defined as the average achievable data rate of a user per unit bandwidth:

$$\bar{\eta}_{SE} = \int_{V_0} \int_0^\infty \log_2(1+\gamma) P_\gamma(\gamma) p(\mathbf{r}) d\gamma d\mathbf{r}. \tag{8}$$

The worst-case link SE corresponds to the scenario when users are located at selected points at the edge of a cell, as shown in Fig.1, and can be written as $\eta_{SE,w} = \eta_{SE}(R,0,0)$. Similarly, the best-case link SE, denoted by $\eta_{SE,b}$, corresponds to the scenario when users are closest to the UAV-gNB at R_0 distance and thus $\eta_{SE,b} = \eta_{SE}(R_0,0,0)$.

E. Spectrum Utilization Efficiency

We introduce the concept of *volume SUE* for fully loaded systems in which the cell's resources are fully used and the number of interferers is constant and equal to N_I. SUE is particularly useful for system design and spectrum management as it helps in optimizing the allocation and reuse of frequencies thereby enhancing the overall performance of the network [3], [8]. For a given communication system in 3D space, SUE can be defined as the ratio of the average achievable sum rate of the system per unit bandwidth to the volume of the system:

$$\eta_{SUE} = \frac{C_T}{B_T V} \tag{9}$$

where C_T is the average achievable sum rate of users in the system conditioned on the user locations, B_T is the total bandwidth allocated to the system and V is the total volume of the communication system in 3D space. Here, $C_T = N_{CT} \sum_{k=1}^{N_s} \bar{C}_k$ where N_{CT} is the number of cells in the system and N_s is the number of users in a cell and $B_T = N N_c B$. Further, $V = N_{CT} V_0$ where V_0 is the volume of a frequency reuse cell. Hence, (9) can be rewritten as

$$\eta_{SUE} = \frac{N_{CT} \sum_{k=1}^{N_s} \bar{C}_k}{N N_c B N_{CT} V_0} = \frac{\sum_{k=1}^{N_s} \bar{C}_k}{(N_c B)(N V_0)} \tag{10}$$

where NV_0 represents the volume of a frequency reuse cluster. Since frequencies are reused at a distance D, the volume covered by one of these partitions is roughly $\frac{4}{3}\pi(D/2)^3$. Therefore, the SUE can be written as

$$\eta_{SUE} = \frac{\sum_{k=1}^{N_s} \bar{C}_k}{\frac{4}{3} N_c B \pi (D/2)^3}. \tag{11}$$

Using (6), (11) can be expressed as:

$$\eta_{SUE}(\mathbf{r}) = \frac{6 \sum_{k=1}^{N_s} N_{c,k}}{N_c \pi D_u^3 R^3} \int_0^\infty \log_2(1+\gamma) P_\gamma(\gamma) d\gamma \tag{12}$$

where D_u is the normalized frequency reuse distance where $D_u = D/R$. For a fully loaded system, (12) simplifies to:

$$\eta_{SUE}(\mathbf{r}) = \frac{6}{\pi D_u^3 R^3} \int_0^\infty \log_2(1+\gamma) P_\gamma(\gamma) d\gamma. \tag{13}$$

Average SUE of a system in 3D space is obtained by averaging over the user distribution and can be expressed as:

$$\bar{\eta}_{SUE} = \int_{V_0} \int_0^\infty \frac{6}{\pi D_u^3 R^3} \log_2(1+\gamma) P_\gamma(\gamma) p(\mathbf{r}) d\gamma d\mathbf{r}. \tag{14}$$

As with link SE, the worst-case and best-case SUEs can be written as $\eta_{SUE,w} = \eta_{SUE}(R,0,0)$ and $\eta_{SUE,b} = \eta_{SUE}(R_0,0,0)$.

III. Effect of the path loss analysis

In this section, we derive analytical expressions for the link SE and SUE of fully loaded systems under the free-space path loss model. Note that, the pathloss $PL(r)$ in dB at a distance r can be written as

$$PL(r) = PL_{ref}(r_0) + 10\alpha \log_{10}(r/r_0) \tag{15}$$

where $PL_{ref}(r_0)$ is a path loss in decibels (dB) at the reference distance r_0 and α is the path loss exponent. Assuming equal transmit powers P_0, the receiver antenna gains G_r and the transmit antenna gains G_t for the desired

UAV-gNB and all co-channel UAV-gNBs, the SIR of a user located at $\mathbf{r}$ can be simplified to:

$$\gamma = \frac{S_D(r)}{S_I} = \frac{r^{-\alpha}}{\sum_{i=1}^{N_I} r_i^{-\alpha}} \tag{16}$$

where $r_i = R\sqrt{D_u^2 + (r/R)^2 - 2D_u(r/R)\cos\beta_i}$, β_i is the angle at the desired UAV-gNB measured between i-th interference and user located at $\mathbf{r}$. Then, the average, worst-case, and best-case link SE of a UAV user under pathloss model can be written as

$$\bar{\eta}_{SE} = \int_{V_0} \log_2\left(1 + \frac{r^{-\alpha}}{\sum_{i=1}^{N_I} r_i^{-\alpha}}\right) p(\mathbf{r}) d\mathbf{r}, \tag{17}$$

$$\eta_{SE,w} = \log_2\left(1 + \frac{R^{-\alpha}}{\sum_{i=1}^{N_I} r_{i,w}^{-\alpha}}\right) \tag{18}$$

and

$$\eta_{SE,b} = \log_2\left(1 + \frac{R_0^{-\alpha}}{\sum_{i=1}^{N_I} r_{i,b}^{-\alpha}}\right), \tag{19}$$

where $r_{i,w} = R\sqrt{D_u^2 + 1 - 2D_u\cos\beta_{i,w}}$, $r_{i,b} = \sqrt{R^2D_u^2 + R_0^2 - 2RD_uR_0\cos\beta_{i,b}}$ and $\beta_{i,w}$ and $\beta_{i,b}$ corresponds to worst-case and best case scenario β_i, respectively. It is evident from (17), (18) and (19) that increasing the normalized frequency reuse distance D_u reduces the interference experienced by a user, thereby increasing the SIR. Consequently, average, worst-case, and best-case link SE increase with an increase in D_u. Similarly, average, worst-case, and best-case SUE can be expressed as

$$\bar{\eta}_{SUE} = \frac{6}{\pi D_u^3 R^3} \int_{V_0} \log_2\left(1 + \frac{r^{-\alpha}}{\sum_{i=1}^{N_I} r_i^{-\alpha}}\right) p(\mathbf{r}) d\mathbf{r} \tag{20}$$

$$\eta_{SUE,w} = \frac{6}{\pi D_u^3 R^3} \log_2\left(1 + \frac{R^{-\alpha}}{\sum_{i=1}^{N_I} r_{i,w}^{-\alpha}}\right) \tag{21}$$

and

$$\eta_{SUE,b} = \frac{6}{\pi D_u^3 R^3} \log_2\left(1 + \frac{R_0^{-\alpha}}{\sum_{i=1}^{N_I} r_{i,b}^{-\alpha}}\right), \tag{22}$$

respectively. It can be observed from equations (20), (21), and (22) that while $\log(.)$ term increases with the normalized frequency reuse distance D_u, the term $1/D_u^3$ decreases with D_u. Depending on which term dominates, the average, worst-case, and best-case SUE may either increase or decrease.

IV. Effect of log-normal shadowing analysis

In this section, we analyze the SUE of a fully loaded cellular system where signals from both desired and interfering UAV-gNBs are affected by log-normal shadowing superimposed on path loss. The log-normal path loss model characterizes the signal attenuation over a given distance r and is expressed in decibels (dB) as [6]:

$$PL(r) = PL_{ref}(r_0) + 10\alpha\log_{10}(r/r_0) + X_\delta \tag{23}$$

where X_δ represents the log-normal shadowing component, modeled as a Gaussian random variable with zero mean and variance σ_δ^2. Hence, using (2), the SIR of a user located at $\mathbf{r}$ becomes

$$\gamma = \frac{e^{-(10\alpha\log_{10}(r/r_0) + X_{D,\delta})/\xi}}{\sum_{i=1}^{N_I} e^{-(10\alpha\log_{10}(r_i/r_0) + X_{i,\delta})/\xi}} \tag{24}$$

where $\xi = 10/\ln(10)$.

The desired UAV-gNB's pathloss is assumed to be log-normally shadowed according to (23) with mean power μ_d and standard deviation σ_d. There are N_I mutually independent log-normally shadowed interferers, each with mean μ_i and standard deviation σ_i. The interferers $X_{i,\delta}$ are assumed to be homoscedastic random variables so that

$$\sigma_i = \sigma_0 \quad i = 1, 2, 3, ..., N_I. \tag{25}$$

Conditioned on the user location $\mathbf{r}$, interference power is a sum of independent log-normal random variables. Although there is no exact closed-form expression for the PDF of a sum of log-normally distributed random variables, it can reasonably be approximated by another log-normal distribution [9], [10]. For instance, according to the Fenton-Wilkinson method, the logarithmic mean μ_I and the logarithmic variance σ_I^2 of a sum of N_I log-normal random variables with same variances can be found by matching the first and second order moments, which yields

$$\mu_I = \frac{-\xi}{2}\ln\left((e^{\sigma_0^2/\xi^2} - 1)\frac{\sum_{i=1}^{N_I} e^{-20\alpha\log_{10}(r_i/r_0)/\xi}}{\left(\sum_{i=1}^{N_I} e^{-10\alpha\log_{10}(r_i/r_0)/\xi}\right)^2} + 1\right) + \frac{\sigma_0^2}{2\xi} + \xi\ln\left(\sum_{i=1}^{N_I} e^{-10\alpha\log_{10}(r_i/r_0)/\xi}\right) \tag{26}$$

and

$$\sigma_I^2 = \xi^2\ln\left((e^{\sigma_0^2/\xi^2} - 1)\frac{\sum_{i=1}^{N_I} e^{-20\alpha\log_{10}(r_i/r_0)/\xi}}{\left(\sum_{i=1}^{N_I} e^{-10\alpha\log_{10}(r_i/r_0)/\xi}\right)^2} + 1\right). \tag{27}$$

We can further simplify (26) and (27) as

$$\mu_I = \frac{-\xi}{2}\ln\left(\frac{(e^{\sigma_0^2/\xi^2} - 1)\sum_{i=1}^{N_I} r_i^{-2\alpha}}{\left(\sum_{i=1}^{N_I} r_i^{-\alpha}\right)^2} + 1\right) + \frac{\sigma_0^2}{2\xi} + \xi\ln\left(\sum_{i=1}^{N_I}\left(\frac{r_i}{r_0}\right)^{-\alpha}\right) \tag{28}$$

and

$$\sigma_I^2 = \xi^2\ln\left((e^{\sigma_0^2/\xi^2} - 1)\frac{\sum_{i=1}^{N_I} r_i^{-2\alpha}}{\left(\sum_{i=1}^{N_I} r_i{}^{-\alpha}\right)^2} + 1\right). \tag{29}$$

The SIR γ, being the ratio of two log-normal random variables, also follows a log-normal distribution [9]. The logarithmic mean μ_γ and logarithmic variance σ_γ^2 of γ can thus be expressed as:

$$\mu_\gamma(\mathbf{r}) = -10\alpha\log_{10}(r/r_0) - \mu_I, \tag{30}$$

$$\sigma_\gamma^2(\mathbf{r}) = \sigma_d^2 + \sigma_I^2. \tag{31}$$

Therefore the PDF of SIR γ conditioned on user location $\mathbf{r}$ can be written as:

$$P_\gamma(\gamma) = \frac{\xi}{\sqrt{2\pi}\sigma_\gamma\gamma} e^{-\frac{(\xi\ln(\gamma) - \mu_\gamma)^2}{2\sigma_\gamma^2}}. \tag{32}$$

Then average achievable rate of k-th user at location $\mathbf{r}$ can be expressed as:

$$\bar{C}_k(\mathbf{r}) = \int_0^\infty C_k(\mathbf{r}) P_\gamma(\gamma) d\gamma \tag{33}$$

where $C_k(\mathbf{r})$ is the achievable rate of k-th user at location $\mathbf{r}$ given by (6). Hence,

$$\bar{C}_k(\mathbf{r})=\frac{\xi N_{c,k}B}{\sqrt{2\pi}\sigma_\gamma \ln(2)}\int_0^\infty \frac{\ln(1+\gamma)}{\gamma} e^{-\frac{(\xi\ln(\gamma)-\mu_\gamma)^2}{2\sigma_\gamma^2}} d\gamma. \quad (34)$$

We may use the inequality:

$$\ln(\gamma+1) \le \ln(\gamma)+1/\gamma \quad (35)$$

to obtain an upper bound to the above average achievable rate:

$$\bar{C}_{k,ub}(\mathbf{r}) = \frac{N_{c,k}B}{\ln(2)}\left(\frac{\mu_\gamma}{\xi}+e^{\frac{\sigma_\gamma^2}{2\xi^2}-\frac{\mu_\gamma}{\xi}}\right). \quad (36)$$

To obtain a lower bound, we use the inequalities

$$\ln(\gamma+1) \ge \begin{cases} \ln(\gamma)+1-\gamma & 0\le\gamma\le 1 \\ \ln(\gamma) & \gamma\ge 1, \end{cases} \quad (37)$$

so that

$$\bar{C}_{k,lb}(\mathbf{r})=\frac{N_{c,k}B}{\ln(2)}\left(\frac{\mu_\gamma}{\xi}+Q\left(\frac{\mu_\gamma}{\sigma_\gamma}\right)-e^{\frac{\sigma_\gamma^2}{2\xi^2}+\frac{\mu_\gamma}{\xi}}Q\left(\frac{\mu_\gamma}{\sigma_\gamma}+\frac{\sigma_\gamma}{\xi}\right)\right) \quad (38)$$

where $Q(x)=(1/\sqrt{2\pi})\int_x^{+\infty} e^{\frac{-t^2}{2}}dt$.

Now, the link SE of a user at location $\mathbf{r}$ can be written as

$$\eta_{SE}(\mathbf{r}) = \frac{\xi\log_2(e)}{\sqrt{2\pi}\sigma_\gamma}\int_0^\infty \frac{\ln(1+\gamma)}{\gamma} e^{-\frac{(\xi\ln(\gamma)-\mu_\gamma)^2}{2\sigma_\gamma^2}} d\gamma \quad (39)$$

so that the average link SE is

$$\bar{\eta}_{SE} = \int_{V_0} \eta_{SE}(\mathbf{r})p(\mathbf{r})d\mathbf{r}. \quad (40)$$

However, given (39) has no closed-form solution, $\eta_{SE}(\mathbf{r})$ can't be directly evaluated. Using (36) and (38), we can express upper and lower bounds for link SE of a user at location $\mathbf{r}$ as

$$\eta_{SE,ub}(\mathbf{r}) = \frac{1}{\ln(2)}\left(\frac{\mu_\gamma}{\xi}+e^{\frac{\sigma_\gamma^2}{2\xi^2}-\frac{\mu_\gamma}{\xi}}\right) \quad (41)$$

and

$$\eta_{SE,lb}(\mathbf{r})=\log_2(e)\left(\frac{\mu_\gamma}{\xi}+Q\left(\frac{\mu_\gamma}{\sigma_\gamma}\right)-e^{\frac{\sigma_\gamma^2}{2\xi^2}+\frac{\mu_\gamma}{\xi}}Q\left(\frac{\mu_\gamma}{\sigma_\gamma}+\frac{\sigma_\gamma}{\xi}\right)\right), \quad (42)$$

respectively. Hence, the upper and lower bounds on average link SE are given by

$$\bar{\eta}_{SE,ub} = \int_{V_0} \eta_{SE,ub}(\mathbf{r})p(\mathbf{r})d\mathbf{r}, \quad (43)$$

and

$$\bar{\eta}_{SE,lb} = \int_{V_0} \eta_{SE,lb}(\mathbf{r})p(\mathbf{r})d\mathbf{r}, \quad (44)$$

respectively. To determine an approximation to the worst-case scenario for link SE $\eta_{SE,w}$, we compute the lower bound of $\eta_{SE,w}$ as $\eta_{SE,w,lb} = \eta_{SE,lb}(R,0,0)$. Similarly, the upper bound on $\eta_{SE,b}$ can be calculated as $\eta_{SE,b,ub} = \eta_{SE,ub}(R_0,0,0)$.

The SUE in 3D space under log-normal shadowing can be expressed in terms of $\bar{C}_k(\mathbf{r})$ using the definition in (11) as

$$\eta_{SUE}(\mathbf{r}) = \frac{\sum_{k=1}^{N_s}\bar{C}_k(\mathbf{r})}{\frac{4}{3}N_cB\pi(D/2)^3} \quad (45)$$

which becomes

$$\eta_{SUE}(\mathbf{r}) = \frac{6\xi\int_0^\infty \frac{\ln(1+\gamma)}{\gamma} e^{-\frac{(\xi\ln(\gamma)-\mu_\gamma)^2}{2\sigma_\gamma^2}} d\gamma}{\sqrt{2\pi}\sigma_\gamma\ln(2)\pi D_u^3R^3}. \quad (46)$$

So that the average SUE can be written as

$$\bar{\eta}_{SUE} = \int_{V_0} \eta_{SUE}(\mathbf{r})p(\mathbf{r})d\mathbf{r}. \quad (47)$$

Similar to $\eta_{SE}(\mathbf{r})$, given (46) has no closed-form solution, we can obtain upper and lower bounds for $\eta_{SUE}(\mathbf{r})$ using (36) and (38) as

$$\eta_{SUE,ub}(\mathbf{r}) = \frac{6}{\ln(2)\pi D_u^3R^3}\left(\frac{\mu_\gamma}{\xi}+e^{\frac{\sigma_\gamma^2}{2\xi^2}-\frac{\mu_\gamma}{\xi}}\right) \quad (48)$$

and

$$\eta_{SUE,lb}(\mathbf{r})=\frac{6\log_2(e)}{\pi D_u^3R^3}\left(\frac{\mu_\gamma}{\xi}+Q\left(\frac{\mu_\gamma}{\sigma_\gamma}\right)-e^{\frac{\sigma_\gamma^2}{2\xi^2}+\frac{\mu_\gamma}{\xi}}Q\left(\frac{\mu_\gamma}{\sigma_\gamma}+\frac{\sigma_\gamma}{\xi}\right)\right), \quad (49)$$

respectively. Hence, the upper and lower bounds on average SUE are given by

$$\bar{\eta}_{SUE,ub} = \int_{V_0} \eta_{SUE,ub}(\mathbf{r})p(\mathbf{r})d\mathbf{r} \quad (50)$$

and

$$\bar{\eta}_{SUE,lb} = \int_{V_0} \eta_{SUE,lb}(\mathbf{r})p(\mathbf{r})d\mathbf{r}, \quad (51)$$

respectively. We may also obtain the lower bound on the worst-case SUE $\eta_{SUE,w}$ as $\eta_{SUE,w,lb} = \eta_{SUE,lb}(R,0,0)$. For the best-case scenario, the upper bound of $\eta_{SUE,b}$ is $\eta_{SUE,b,ub} = \eta_{SUE,ub}(R_0,0,0)$.

V. Simulation

In this section we use a simulated UAV network in 3D space to demonstrate how closely our analytical approximations agree with such a system. In simulations, we assume $N_s = 30$ number of UAV-UEs in a cell at random locations generated according to the PDF (1). Co-channel UAV-gNBs are positioned according to the frequency reuse plan outlined in Section II-A. Given that there are two distinct frequency reuse distances, we use the average frequency reuse distance for SUE computation as $D = \frac{8D_h+6D_s}{14}$. To determine SUE of a communication system, we first calculate the achievable data rate of a user in the cell using (4). We distribute $N_c = 100$ channels equally among UAV-UEs. Unless specified otherwise, $R_0 = 10m$, $\alpha = 2.5$, $\sigma_0 = 3dB$ and $R = 800m$ [1], [6].

Figure 2 shows the dependence of SUE and link SE on parameters α and R relative to the normalized frequency reuse distance under the pathloss channel model of (15). Figure 2 shows that the analytical expressions for average SUE and average link SE given in (20) and (17), respectively, consistently align with those computed in the simulation. We observe that an increase in normalized frequency reuse distance decreases SUE, while it increases average link SE of the system. To optimize SUE, we can choose the corresponding frequency reuse distance that maximizes SUE in the communication system based on required average link SE. Figure 2 also shows that reducing the cell size increases SUE of the communication system in 3D space. Specifically, Figs. 2 (a) and (b) show an increase in SUE by up to 0.79 $bit/s/Hz/km^3$ for the same D_u, when decreasing the cell radius from $800m$ to $600m$. Additionally, results indicate that larger the exponential path loss α better the SUE due to the reduction in interference power. Comparing Figs. 2 (a) and (c), we observe an increase in SUE by up to $0.19bit/s/Hz/km^3$ when α is increased from 2.5 to 3.

Figure 3 considers the log-normal pathloss channel described in (23). The simulation results fall within the derived

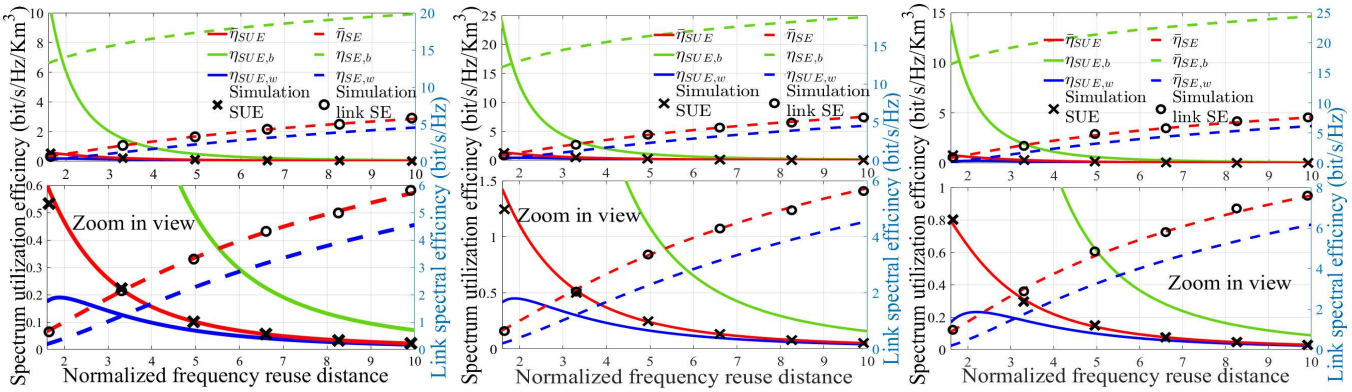

(a) $\alpha = 2.5$, $R = 800m$ (b) $\alpha = 2.5$, $R = 600m$ (c) $\alpha = 3$, $R = 800m$

Fig. 2: SUE and link SE variation with normalized frequency reuse distance ignoring the effects of log-normal shadowing, with both zoomed-in and zoomed-out views in each figure

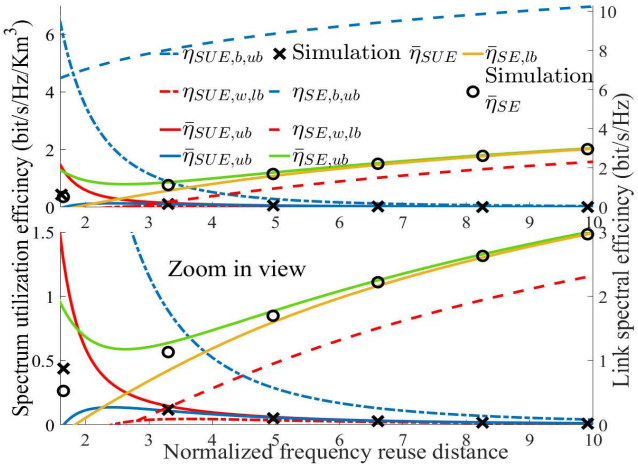

Fig. 3: SUE and link SE variation with normalized frequency reuse distance with log-normal pathloss model, with both zoomed-in and zoomed-out views in each figure

upper and lower bound curves in (50) and (51). Similar to the previous case, the upper and lower bounds indicate that as the normalized frequency reuse distance increases, SUE tends to decrease while average link SE potentially increases. Simulation results validate this trend at least for the specific simulation points considered. However, the computed lower bounds for link SE and SUE fall below zero at lower values of D_u. Since these metrics cannot be negative, the lower bounds are only considered in regions where these are positive.

VI. Conclusion

This paper provides an analysis of SUE and average link SE in 3D UAV communication systems. By examining various pathloss models and dependence of link SE and SUE on key parameters of cell radius and pathloss exponent, we provided valuable insights into performance trade-offs. Simulations validate our theoretical analysis, showing that SUE decreases as the normalized frequency reuse distance D_u increases, while average link SE improves. These findings highlight the importance of carefully selecting the frequency reuse distance to optimize system performance based on specific deployment scenarios and Quality-of-Service (QoS) requirements. We observed that reducing the cell radius R increases the link SE and SUE for the same normalized frequency reuse distances. This improvement stems from the increased number of cells per unit volume. However, achieving this improvement requires greater deployment costs, as additional UAV-gNBs are required to accommodate the increased number of cells. Similarly, increasing the pathloss exponent from 2.5 to 3 resulted in a noticeable improvement in SUE. In scenarios using the log-normal pathloss model, the simulation results were consistent with the theoretical bounds, further reinforcing the soundness of our analytical framework.

This work establishes the groundwork for optimizing frequency reuse in UAV communication networks in 3D space and dynamic spectrum sharing in integrated aerial and ground communication environments.

References

[1] M. Mozaffari *et al.*, "Beyond 5G with UAVs: Foundations of a 3D wireless cellular network," *IEEE Trans. on Wireless Communications*, vol. 18, no. 1, pp. 357–372, 2019.

[2] K. Prabhath and S. K. Jayaweera, "Optimal adaptation of 3D beamformers in UAV networks," in *Fourteenth Int.Conf. on Ubiquitous and Future Networks (ICUFN)*, 2023, pp. 207–212.

[3] I. T. Union, "Definition of spectrum use and efficiency of a radio system," ITU, Recommendation ITU-R SM.1046-1, 1997.

[4] C. K. Armeniakos *et al.*, "Finite point processes in a truncated octahedron-based 3D UAV network," *IEEE Trans. on Vehicular Technology*, vol. 71, no. 7, pp. 7230–43, 2022.

[5] K. Prabhath and S. K. Jayaweera, "Frequency reuse planning in 3D space for DAV swarm communications," in *2023 IEEE 98th Vehicular Technology Conference (VTC2023-Fall)*, 2023, pp. 1–6.

[6] Y. Lyu *et al.*, "A study on radio propagation channel modeling for low altitude UAV," in *IEEE 6th Int. Conf. on Electro. and Communi.Eng.(ICECE)*, 2023, pp. 110–4.

[7] Z. Wei *et al.*, "The performance analysis of spectrum sharing between UAV enabled wireless mesh networks and ground networks," *IEEE Sensors Journal*, vol. 21, no. 5, pp. 7034–7045, 2021.

[8] M. S. Alouini and A. J. Goldsmith, "Area spectral efficiency of cellular mobile radio systems," *IEEE Trans. on Vehi. Tech.*, vol. 48, no. 4, pp. 1047–66, 1999.

[9] J. Wu *et al.*, "Flexible lognormal sum approximation method," in *IEEE Global Telecommunications Conf.*, vol. 6, 2005, pp. 3413–3417.

[10] G. L. Stuber, *Principles of Mobile Communication*. Springer, 2017.